Applications
in Plant Sciences

APPLICATION ARTICLE

Improved image processing for 3D virtual object construction from serial sections reveals tissue patterns in root tips of *Zea mays*

Yasushi Miki[1] | Susumu Saito[1] | Teruo Niki[1] | Daniel K. Gladish[2]

[1]Image Processing Section, MikiOn LLC, 103 Ishikawa Heights, 1737 Hazama-machi, Hachioji, Tokyo 193-0941, Japan

[2]Department of Biology, Miami University, 1601 University Blvd., Hamilton, Ohio 45011, USA

Correspondence

Daniel K. Gladish, Biology Department, Miami University, 1601 University Blvd., Hamilton, Ohio 45011, USA.
Email: gladisdk@miamioh.edu

Abstract

Premise: Previously we described methods for generating three-dimensional (3D) virtual reconstructions of plant tissues from transverse thin sections. Here, we report the applicability of longitudinal sections and improved image-processing steps that are simpler to perform and utilize free applications.

Methods: In order to obtain improved digital images and a virtual 3D object (cuboid), GIMP 2.10 and ImageJ 2.3.0 running on a laptop computer were used. Sectional views of the cuboid and 3D visualization were realized with use of the plug-ins "Volume Viewer" and "3D Viewer" in ImageJ.

Results: A 3D object was constructed and sectional views along several cutting planes were generated. The 3D object consisted of selected tissues inside the cuboid that were extracted and visualized from the original section data, and an animated video of the 3D construct was also produced.

Discussion: Virtual cuboids can be constructed by stacking longitudinal images along the transverse depth direction or stacking transverse images vertically along the organ axis, with both generating similar 3D objects. Which to use depends on the purpose of the investigation: if the vertical cell structures need close examination, the former method may be better, but for more general spatial evaluations or for evaluation of organs over longer tissue distances than can be accommodated with longitudinal sectioning, the latter method should be chosen.

KEYWORDS

3D construction, cell outline extraction, image alignment, serial sections, *Zea mays*

The ability to make unobstructed observations of tissues and cells in three dimensions has long been an ambition of anatomists and histologists, and several methods have already been developed. Non-destructive bio-imaging methods, such as confocal imaging (Gray et al., 1999; Bougourd et al., 2000; Haseloff, 2003; Kitin et al., 2003; Wegel et al., 2005; Buda et al., 2009), optical projection tomography (Lee et al., 2006), X-ray techniques (Stuppy et al., 2003), and nuclear magnetic resonance imaging (Glidewell et al., 1999; Ishida et al., 2000; Mill et al., 2004; Glidewell, 2006), have been successfully applied to generate three-dimensional (3D) images of plant organs and tissues.

Among these methods, confocal microscopy may be the most useful for observing plant tissue cell structure because it has sufficiently high resolution for cell-by-cell observations and can relatively easily capture digital information for computational manipulation. By systematically changing the depth of focus and acquiring a large number of two-dimensional images, a 3D image can be generated (Gray et al., 1999; Bougourd et al., 2000; Haseloff, 2003; Kitin et al., 2003; Wegel et al., 2005; Buda et al., 2009). There are, however, some limitations; because a focused spot of a laser beam is scanned within a specimen, the useful information is restricted to tissues less than 200 μm thick (Bougourd et al., 2000), as well as by the working distance of the objective lens. Moreover, the specimen must be cleared with chemicals, such as chloral hydrate or xylene, and subsequently stained with a fluorescent staining agent, such as

safranin O (Gray et al., 1999; Kitin et al., 2003) or auramine O (Buda et al., 2009), to allow the high-resolution confocal imaging of individual cells within the tissue. To date, 3D visualizations of tissues or cell structures using a confocal microscope have been limited to a few species (e.g., *Vitis vinifera* L., *Solanum lycopersicum* L., *Arabidopsis thaliana* (L.) Heynh., and *Oryza sativa* L.) or to cultured cells.

Although it is destructive, optical microscopy by physical sectioning can provide high-resolution images and 3D imaging with the aid of a computer (Ogawa et al., 2002; Gubatz et al., 2007), permitting a much wider range of specimen sizes accommodated by the use of different types of microtomes. Ogawa et al. (2002) and Gubatz et al. (2007) investigated relatively large specimens (developing caryopses) but did not analyze individual cells in a tissue. Although tissue preparation, sectioning, staining, image capture, and 3D modeling techniques require some skill and patience (Ourselin et al., 2000; Bussolati et al., 2005; Miki et al., 2020), physical sectioning methods enable the detailed structural analysis of many species and types of plant organs. However, in order to reconstruct accurate 3D images with this method, it is important that the cutting of each thin section causes very limited distortion, and that the contours of cells and tissues are clearly defined.

For previous work, we developed histochemical techniques that enhance contrast and make all cell walls more sharply defined (Niki et al., 2019). We used serial transverse thin sections prepared using those techniques to construct a 3D virtual object for analyzing histogenesis in root tips of teosinte (*Zea mays* L. subsp. *mexicana* (Schrad.) Iltis). For the digital image collection, we added a three-axis coordinate system and addressed the challenge of accurately aligning the resulting digital micrographs by relying on both that system and the alignment of distinctive cell lineages, such as late-maturing metaxylem vessels (LMX). We used a computational approach within the three-axis coordinate system to evaluate and manage the sectioning-induced distortion of the embedding medium. Minor scaling adjustments were made manually in the image management applications when distortion was perceived in a section micrograph (Miki et al., 2020).

A 3D reconstruction of the root-tip tissue of teosinte was successfully obtained using this imaging method and digital image processing technique, which was performed using Photoshop Elements 2018 (Adobe, San Jose, California, USA) and Mathematica version 11 (Wolfram Research, Champaign, Illinois, USA). The 3D object could be virtually sectioned in arbitrary planes and rotated to analyze patterns of tissue development (Miki et al., 2020).

For the current work, we decided to use GIMP version 2.10 (GIMP Development Team, 2018) and ImageJ version 2.3.0 (Rasband, 1997–2014) running on a MacBook laptop computer (Apple, Cupertino, California, USA). These are free open-source applications, and many useful plug-ins are available. "Batch Image Manipulation" and "Export Layers" in GIMP were especially useful for the batch processing of image stacks. Furthermore, "3D Viewer" and "Volume Viewer" in ImageJ were useful for the 3D construction and visualization, and the "Find Maxima" tool in ImageJ was excellent for cell-wall outline extraction from the original images. Taking advantage of these features allowed us to develop a new, simpler approach to mitigate any sectioning-induced distortion and to align serial-section micrographs in a digital stack suitable for generating a 3D virtual reconstruction of the original root tissues.

MATERIALS AND METHODS

Plant materials

The cultivation methods were modified after Gladish and Niki (2000). Teosinte seeds (*Zea mays* subsp. *mexicana*) from Snow Brand Seed (Sapporo, Japan) were surface-sterilized for 5 min in 10% (v/v) household chlorine bleach with 10 drops of Tween 20 surfactant (Sigma-Aldrich, Burlington, Massachusetts, USA) per liter, then rinsed in sterile distilled water. Twenty seeds were sown in each of three 1-L beakers containing autoclave-sterilized, moistened vermiculite, and then placed in a continuously dark growth chamber at a constant temperature of 20°C for four days.

Thin sections for light microscopy

Procedures for light microscopy were modified from Niki et al. (1995). Root-tip segments were excised from the selected roots (apical 1.0 cm), immediately immersed in 4% (w/v) paraformaldehyde fixative in 0.1 M phosphate buffer, and shaken gently overnight at room temperature. Following fixation, the specimens were rinsed in buffer, dehydrated by ethanol series, and embedded in Technovit 7100 resin (Heraeus Kulzer, Wehrheim, Germany). Serial sections were then made longitudinally at a thickness of 1 μm on a Reichert-Nissei UCT ultramicrotome (Leica Microsystems, Wetzlar, Germany).
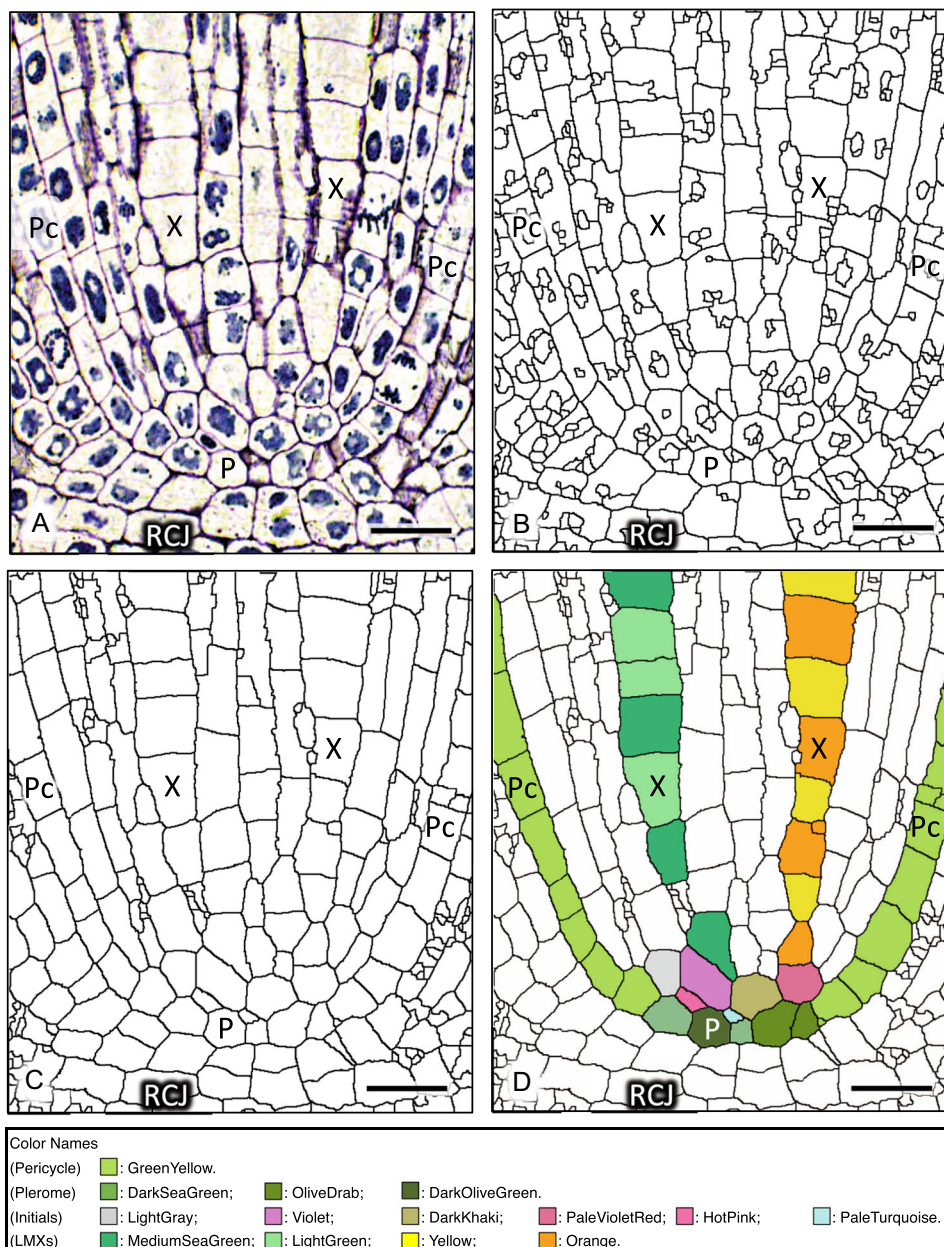
Because apical meristems are cytoplasmically dense and their cell cytoplasms are rich with RNA (Niki et al., 2019; Saito et al., 2019), RNase-treated sections were prepared for light microscopy as described by Niki et al. (2019). Briefly, sections mounted on glass slides were treated with RNase (Sigma-Aldrich) at 60 μg/300 μL in 0.05 M phosphate buffer solution (pH 7.2). This removed RNAs, which would otherwise be heavily stained because of their cytosolic abundance (Majumder et al., 2016) and cause the image to be obscured. The slides were kept in an incubation box at 100% humidity and 37°C for 4 h. After rinsing with distilled water, the sections were stained with 1% (w/v) toluidine blue O (Electron Microscopy Sciences, Hatfield, Pennsylvania, USA) at 45°C for 4 min and rinsed with distilled water.

Photographic imaging of serial sections

Sections were viewed with a Leica DMLB light microscope (Leica Microsystems) equipped with TU Plan Fluor 50× ∞/0 lenses (Nikon, Tokyo, Japan), and photographed with a Canon EOS 5D Mark II digital camera (Canon, Tokyo, Japan), as described by Niki et al. (2019). A total of 60 digital images of serial sections were acquired with a resolution of 5616 × 3744 pixels, which were then reduced by a quarter in both dimensions (1404 × 936 pixels), which corresponds to 270 × 180 µm at 50× magnification.

Preprocessing of images using ImageJ and GIMP

The first preprocessing step was to "extract" cell walls from each original digital image to make the walls clearly delineated and continuous (Figure 1A). The "Find Maxima" plug-in tool in ImageJ was used to extract outlines of cell walls from the dense original digital image data and eliminate cell nuclei (Figure 1B). The second step was to "clean up" the outlined image shown in Figure 1B. Some superfluous objects were erased manually by "breaking" unwanted black lines with white lines, and some cell walls

Color Names					
(Pericycle)	▢: GreenYellow.				
(Plerome)	▢: DarkSeaGreen;	▢: OliveDrab;	▢: DarkOliveGreen.		
(Initials)	▢: LightGray;	▢: Violet;	▢: DarkKhaki;	▢: PaleVioletRed;	▢: HotPink;	▢: PaleTurquoise.
(LMXs)	▢: MediumSeaGreen;	▢: LightGreen;	▢: Yellow;	▢: Orange.	

FIGURE 1 Toluidine blue–stained, RNase-treated median longitudinal sections of the procambial vascular cylinder of a teosinte (*Zea mays* subsp. *mexicana*) root tip. (A) Original image. (B) Outline extraction using the ImageJ plug-in "Find Maxima." (C) Cleaned image with some superfluous objects erased and with some manually redrawn cell walls that vanished during the extraction process. (D) Colorized and color-coded image of (C). P, plerome; Pc, pericycle; RCJ, root cap junction; X, late-maturing metaxylem vessel. Scale bar = 50 µm. The colors used in Figure 1D are listed according to the HTML color names.

that vanished during the Find Maxima extraction process were redrawn manually with black lines using the pencil tool of ImageJ. By redoing the Find Maxima step, unconnected lines were eliminated and the redrawn lines were set to be 1 pixel wide (Figure 1C). The third processing step was to colorize (and color-code) specific cells (LMX, pericycle cells, plerome cells, and their initial cells) using the paint bucket tool in GIMP to distinguish them from other cells (Figure 1D). Color codes and names used in this report were chosen from 140 named colors known as "HTML color names," which are available online (e.g., https://htmlcolors.com/color-names). The color set used in Figure 1D is listed at the bottom of the figure.

The same procedures for extracting cell wall profiles and aligning the images, except for the colorization, were performed for the full set of 60 images (#01 to #60 of the original serial sections) as described above in "Preprocessing" and below in "Alignment." We determined that it was better to perform the colorization procedure after the alignment procedure was completed.

Alignment of the image set using ImageJ and GIMP

Two images of neighboring thin sections were aligned using the following procedure. One image was selected as a reference (#32 of the series in this case) and opened in ImageJ. The outlines of the cell walls were extracted, then cleaned up as described above, and saved as an outlined file. The modified reference image was imported into GIMP, and the image of the adjacent layer (#31) was overlaid onto it as a new translucent layer, so both could be simultaneously seen in the same image window. Transform operations, such as move, scale, skew, and/or their combination, were applied to fit the translucent overlaid image to the reference. These operations were repeated until the images matched each other well, after which the opacity of the overlaid image was restored and the layer was saved as a separate file. ImageJ was used to perform the cell wall outline extraction and clean-up for the aligned image, and the image was saved as an outlined file. This image could then be selected as the new reference, and the same procedure was performed for the next adjacent layer until all images from #32 to #01 were aligned. Then, #32 was used as a reference to align #33 by the same method. This process was repeated in order until all the remaining sections were aligned.

After the alignment procedure was completed, each image was trimmed to 500 × 600 pixels to create a set of 60 images (#01–#60) of the aligned serial sections (Figure 2). The colorization process was then performed as follows. In each figure, separate colors were given to the specified cells (LMX 1, Turquoise/DeepSkyBlue; LMX 2, LightGreen/MediumSea-Green; LMX 3, Yellow/Orange; LMX 4, Red/OrangeRed; pericycle, GreenYellow; plerome, DarkSeaGreen, OliveDrab, and DarkOliveGreen), with alternating cells in each LMX cell file given different but similar colors (e.g., Turquoise/DeepSkyBlue). Several different colors were also given to initial cells. Because some of the images were not usable due to sectioning defects, the image preceding a damaged section was repeated at those places (e.g., #26, #33, #35, and #55 in Figure 2) to preserve the original tissue dimensions.

RESULTS

Construction of the 3D object and its sectional views

By stacking the aligned longitudinal image sections shown in Figure 2 along the depth direction, a 3D virtual object (cuboid) was constructed (Figure 3A). The dimensions of the cuboid were 500 (x) × 600 (y) × 60 (z) pixels. The pixel sizes along the x-, y-, and z-axes were 0.192 μm, 0.192 μm, and 1 μm, respectively. To preserve the original dimensions, the size along the z-direction was multiplied by 5.2 (=1/0.192).

The ImageJ plug-in "Volume Viewer" provided a wide variety of sectional views of the cuboid. Some examples are shown in Figure 3, where c, d, and e indicate the cutting planes of the cuboid (Figure 3B). A sectional view of plane c ($z = 34$ pixels) is shown in Figure 3C, and digitally processed virtual images of the planes d ($x = 188$ pixels) and e ($x = 342$ pixels) are shown in Figures 3D and 3E, respectively.

Another example of a sectional view from the same virtual cuboid that illustrates the utility of this method is shown in Figure 4; Figure 4A displays a sectional view along the cutting plane a–a′ from Figure 4B ($z_a = 5$ pixels, $z_{a'} = 32$ pixels), and Figure 4B displays a sectional view along the cutting plane b–b′ from Figure 4A ($x = 238$ pixels). The cutting plane a–a′ was set almost vertical and perpendicular to the plane (Figure 4B), but inclined to an angle of 13° so that the plane intersected all the blue LMX cells in Figure 4B. As a result, all the cell connections of the LMX can be clearly observed.

The transverse sectional images of the cuboid are shown at several positions of cutting xz-planes in Figure 5, where Figure 5A shows an image of the top plane ($y = 0$ pixels), and Figure 5B–D show sectional images at heights $y = 217$ pixels (Figure 5B), $y = 461$ pixels (Figure 5C), and $y = 493$ pixels (Figure 5D). Four colored cells, Red/Orange/Light-Green/Turquoise (Figure 5A) and OrangeRed/Yellow/LightGreen/DeepSkyBlue (Figure 5B), are marked as "X" to indicate the corresponding LMX elements. In Figure 5C, several colored cells (Violet, PaleVioletRed, HotPink, MediumPurple, LightSkyBlue, Khaki, and DarkKhaki) were located surrounding the central (PaleTurquoise) cell; these were likely initial cells because of their position in the vascular initials layer basipetal to the plerome (Saito et al., 2019). The set of cells that we labeled with three similar colors (DarkSeaGreen, OliveDrab, and DarkOlive-Green) were identified as the plerome histogen of this root tip (Figure 5D).
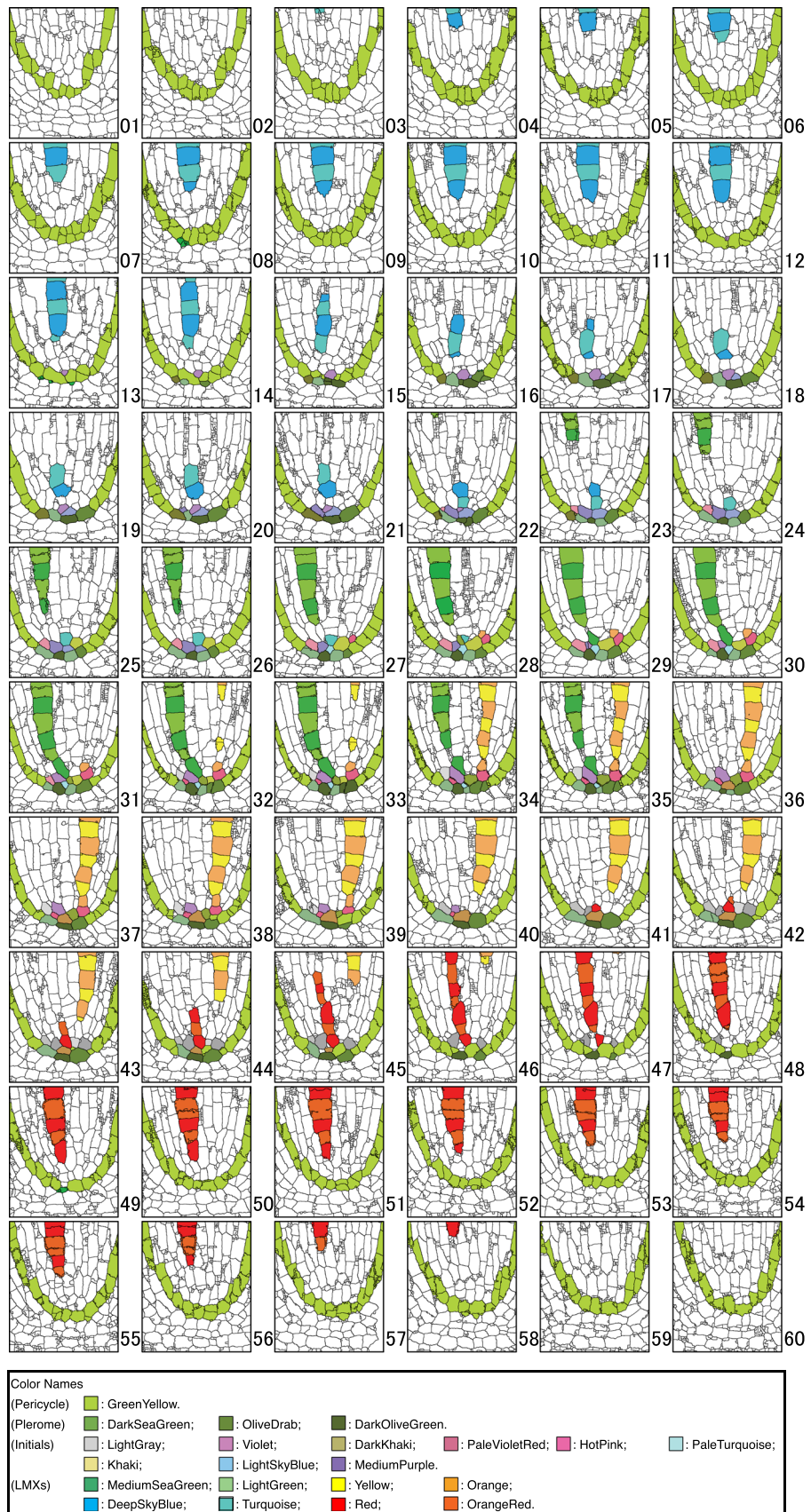
Color Names

(Pericycle) ▢ : GreenYellow.

(Plerome) ▢ : DarkSeaGreen; ▢ : OliveDrab; ▢ : DarkOliveGreen.

(Initials) ▢ : LightGray; ▢ : Violet; ▢ : DarkKhaki; ▢ : PaleVioletRed; ▢ : HotPink; ▢ : PaleTurquoise;

▢ : Khaki; ▢ : LightSkyBlue; ▢ : MediumPurple.

(LMXs) ▢ : MediumSeaGreen; ▢ : LightGreen; ▢ : Yellow; ▢ : Orange;

▢ : DeepSkyBlue; ▢ : Turquoise; ▢ : Red; ▢ : OrangeRed.

FIGURE 2 (See caption on next page)

3D construction of selected tissues

A virtual 3D object comprising LMX vessels, initial cells, and the plerome was produced from the set of images shown in Figure 2 using the ImageJ plug-in "3D Viewer" (Figure 6). The White and GreenYellow colors of each image were changed to Black (Figure 6A, B). The stacked images were imported into ImageJ. Because the pixel sizes along the x-, y-, and z-axes were 0.192 μm, 0.192 μm, and 1 μm, respectively, as described above, the "Z Scale" value in
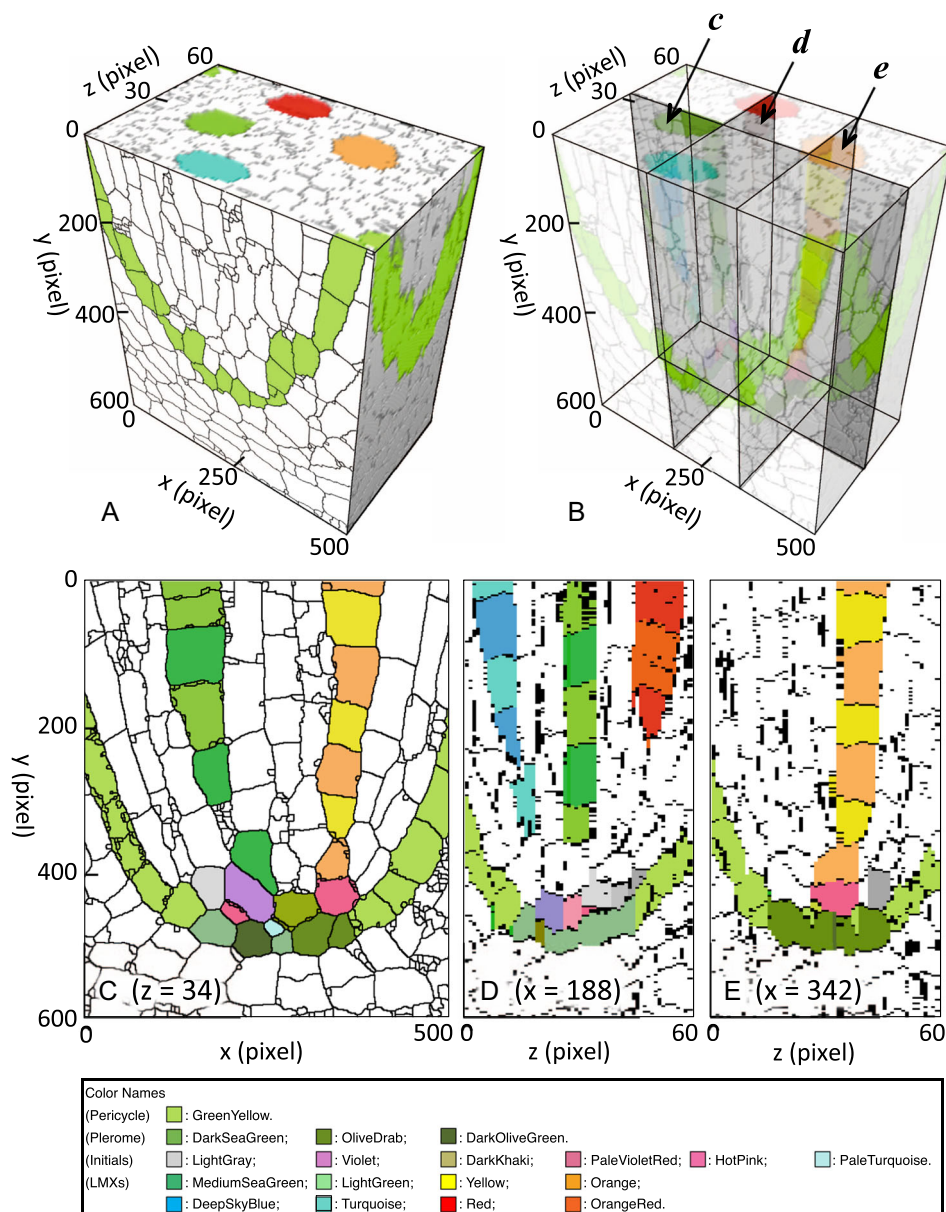
FIGURE 3 Possible manipulations of a digitally constructed virtual object. (A) 3D object (cuboid) constructed by stacking 60 layers of the sections shown in Figure 2 along the depth direction. The dimension of the cuboid is 500 (x) × 600 (y) × 60 (z) pixels. The pixel sizes along the x-, y-, and z-axes are 0.192 μm, 0.192 μm, and 1 μm, respectively. For the preservation of the original dimensions, the size along z-direction was multiplied by 5.2 (=1/0.192). (B) Cuboid shown in (A) "cleared" to show cutting planes *c*, *d*, and *e* of the 3D object. (C) Sectional view of the plane *c* (z = 34 pixels). This is layer #34, shown in Figure 2. (D) Sectional view of the plane *d* (x = 188 pixels). (E) Sectional view of the plane *e* (x = 342 pixels). (D) and (E) are digitally processed virtual images constructed using the ImageJ plug-in "Volume Viewer."

FIGURE 2 Set of 60 renumbered images (#01–#60) of the aligned serial sections. Separate colors were given to specified cells (late-maturing metaxylem [LMX]) 1, Turquoise/DeepSkyBlue; LMX 2, LightGreen/MediumSeaGreen; LMX 3, Yellow/Orange; LMX 4, Red/OrangeRed; pericycle, GreenYellow; plerome, DarkSeaGreen, OliveDrab, and DarkOliveGreen), and alternating cells in each LMX cell file were given different but similar colors (e.g., Turquoise/DeepSkyBlue). Several different colors were also given to initial cells.
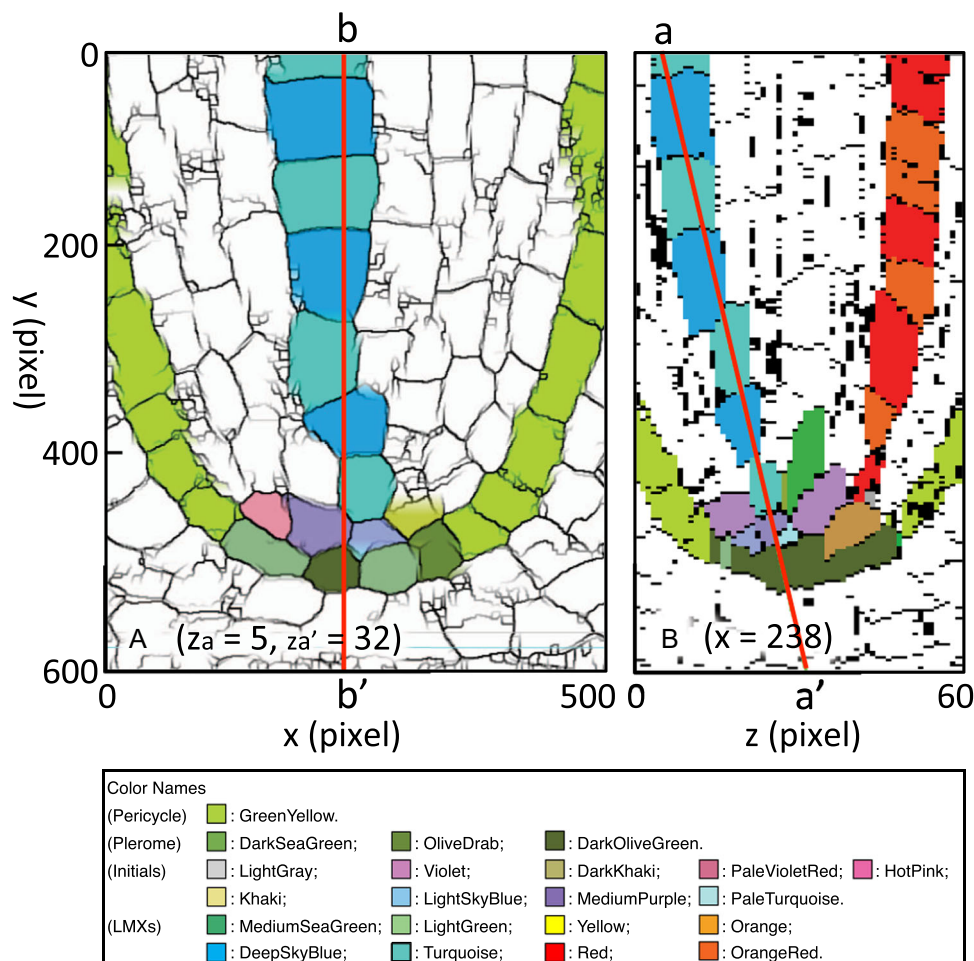
FIGURE 4 Manipulating virtual sectioning of a 3D cuboid for structural analysis. (A) Digitally processed sectional view of the cutting plane taken along the line a–a′ in (B) (z_a = 5 pixels, $z_{a'}$ = 32 pixels). All the cell connections of the blue late-maturing metaxylem (LMX) cells can be clearly observed. (B) Sectional view along a cutting plane b–b′ in (A) (x = 238 pixels). The line a–a′ shows a cutting plane perpendicular to the figure and inclined to an angle of 13°, so that the plane intersects all the blue LMX cells.

ImageJ was changed to 5.2 (=1/0.192) to adjust the pixel size. A new set of images was created automatically by interpolating the original images by the factor of the z-scale value. By selecting the 3D Viewer, a new 3D object was created (Figure 6C). This object can be viewed in any orientation, and can also be seen as an animated movie (Video S1).

DISCUSSION

In morphological and histological studies, it is important to observe tissue sites not only as locally isolated elements, but also as related components of whole structures. To this end, 3D observations are effective and can be useful for linking the structure and function of tissues. Various tools have been developed for this purpose (Haseloff, 2003; Haase et al., 2022), but 3D images have only been realized for a relatively small number of plant species, including *Arabidopsis* (Haseloff, 2003; Truernit et al., 2008), rice (*Oryza sativa*; Ogawa et al., 2002), maize (*Zea mays* subsp.

mexicana; Miki et al., 2020), a woody tree tissue (*Kalopanax pictus* (Thunb.) Nakai; Kitin et al., 2003), and grape (*Vitis vinifera*) and tomato (*Solanum lycopersicum*) fruit (Gray et al., 1999; Buda et al., 2009, respectively). These were obtained mainly in relatively small tissue regions (such as root tips, embryos, epidermis, or vascular bundles). These research samples were mainly limited by the characteristics of the instruments used, and there is no one-size-fits-all instrument or method for any kind of observation. The appropriate method must be determined to achieve the purpose of each project.

Computer applications used

For the present study to evaluate histogenesis in root procambium development, we elected to use GIMP version 2.10 and ImageJ version 2.3.0 instead of the expensive applications we used in previous work (Miki et al., 2020). These are open-source applications, with many useful plug-ins. We used "Batch Image Manipulation" and "Export
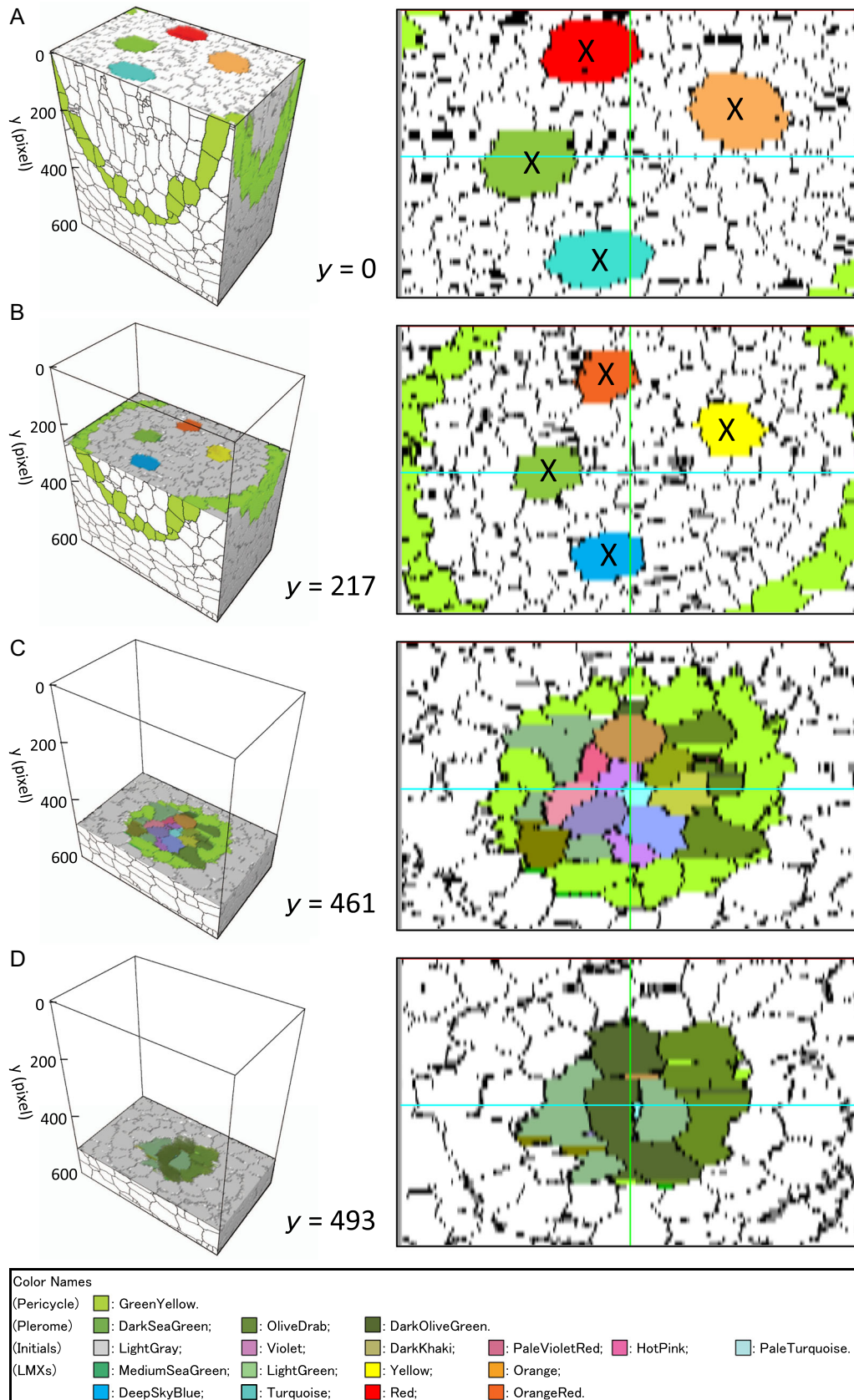
Color Names

(Pericycle)
- : GreenYellow.

(Plerome)
- : DarkSeaGreen;
- : OliveDrab;
- : DarkOliveGreen.

(Initials)
- : LightGray;
- : Violet;
- : DarkKhaki;
- : PaleVioletRed;
- : HotPink;
- : PaleTurquoise.

(LMXs)
- : MediumSeaGreen;
- : LightGreen;
- : Yellow;
- : Orange;
- : DeepSkyBlue;
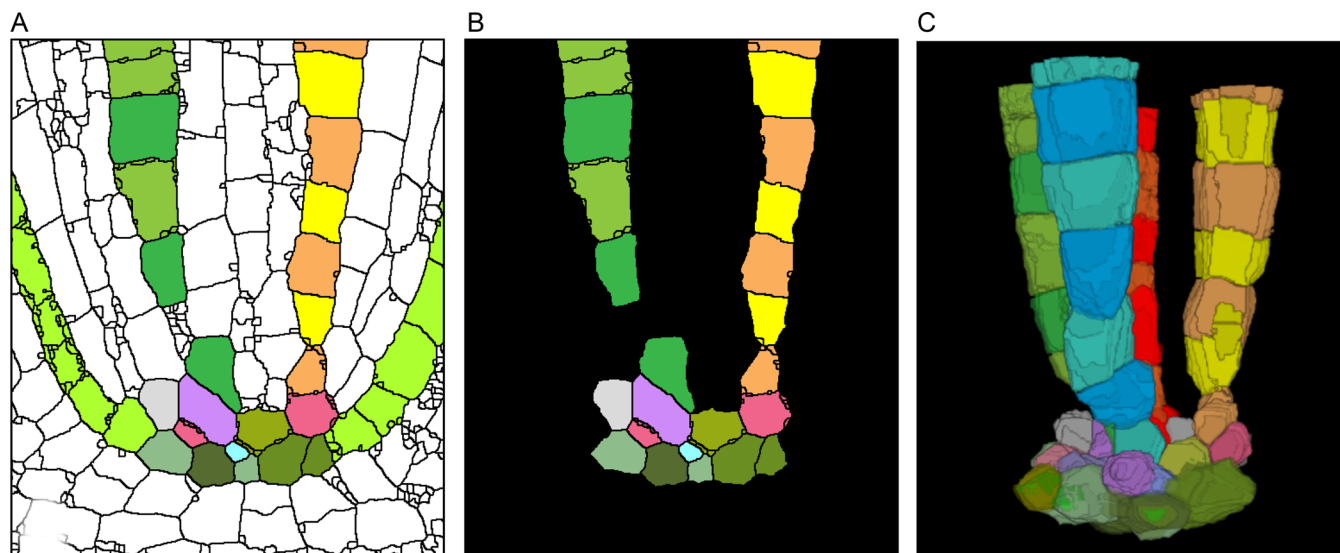- : Turquoise;
- : Red;
- : OrangeRed.

FIGURE 5   (See caption on next page)

FIGURE 6 Generating a virtual 3D object. (A) An original colorized image. (B) Image after the color exchange procedure. White and GreenYellow colors were changed to Black to make them transparent. (C) Virtual 3D object constructed with use of "3D Viewer" in ImageJ.

Layers" in GIMP for batch processing image stacks, and "3D Viewer" and "Volume Viewer" in ImageJ for 3D construction and visualization. In particular, "Find Maxima" in ImageJ enabled the automatic outline extraction; this function was not supported in Mathematica, which we used previously (Miki et al., 2020). Furthermore, programming knowledge or technique is not required for any of the procedures we propose here.

Extracting outlines of cells in photo images and coloring cells

Ourselin et al. (2000) developed a program for registering serial section images of the mouse brain, which may also be useful for the study of plant embryo sections; however, their complicated mathematical method was not used here because our section images (cell walls like a meshwork) are not compatible with their proposed structural image processing method. We manually aligned the images using a much simpler method.

We used the tool "Find Maxima" in ImageJ, which extracts closed curves and removes unconnected lines, to obtain sharply outlined cell structures (Figure 1B). In some cases, researchers must manually add lines to connect/complete cell walls present in the original image that were lost during image processing or, conversely, break superfluous lines from internal cell structures to remove them

(Figure 1C). Although such operations are required, it is worth mentioning that this tool significantly reduced the time and effort required to complete the outline extraction. Furthermore, because the obtained images were sometimes simplified to black and white, the coloring process for specified cells only required the use of the bucket tool in GIMP. The colored cells (plerome, pericycle, xylem vessel elements, and meristematic initials) clearly showed the patterns of cell organization in the root tip (Figure 1D). This coloring procedure made the root structures easily distinguishable when observed as a 3D object (Figure 6), and the slight color differences of the alternating cells in the LMX file made it easier to distinguish the individual cells in the virtual sections (Figures 4, 5).

Sectional views and animation of a 3D object

The "Volume Viewer" provided a wide variety of sectional views, including longitudinal sections (Figure 3C–E), the inclined longitudinal section (Figure 4), and transverse sections (Figure 5). The inclined image might be the best example that the present work can provide. It shows detailed cell connections and highlights the versatility of the current method to reveal perspectives that would otherwise be unobservable. As described above, the "3D Viewer" in ImageJ can generate 3D virtual objects that can be observed from an arbitrary viewpoint, and furthermore, can be

FIGURE 5 Positions of the cutting *xz*-planes showing transverse layer images of the virtual 3D object. (A) Top plane of the object ($y = 0$ pixels). The four colored cells (Red, Orange, LightGreen, and Turquoise) are late-maturing metaxylem (LMX) cells. (B) Image at height $y = 217$ pixels. (C) Image at height $y = 461$ pixels. Initial cells colored with several colors (Violet, PaleVioletRed, HotPink, MediumPurple, LightSkyBlue, Khaki, and DarkKhaki) are located surrounding the central PaleTurquoise cell. (D) Image at height $y = 493$ pixels. The set of olive-colored (DarkSeaGreen, OliveDrab, and DarkOliveGreen) cells form the plerome.

animated, offering insight into the cell-to-cell relationships and tissue structure (Video S1).

Longitudinal sectioning and transverse sectioning

In the present report, the cuboid was constructed by stacking the set of longitudinal images along the depth (transverse) direction, whereas the cuboid in the previous report (Miki et al., 2020) was constructed by stacking the set of transverse images vertically along the organ axis. Both of these approaches could generate similar 3D objects (e.g., a set of LMXs); the former could more clearly show horizontal virtual images, whereas the latter could more clearly show vertical virtual images. The difference between these approaches was the resolution (μm/pixel) along the three directions (x, y, z) shown in Figure 3. The longitudinal image approach used in the present study resulted in pixels 0.192 μm, 0.192 μm, and 1 μm in size, respectively, while those of the previous transverse image approach had pixels 0.192 μm, 1 μm, and 0.192 μm in size, respectively. Which technique to use depends on the purpose of the investigation; if one intends to examine the axially oriented cell and tissue structures more closely, the method based on longitudinal sections may be better, otherwise the method based on transverse sections should be chosen.

Concluding remarks

Many tools have been developed for observing and analyzing tissue structures and constructing 3D images. The physical sectioning method presented here is probably one of the most traditional methods of producing primary graphical information for analyzing anatomical structure in plants; however, combined with the digital image processing technique, this method presents a new and inexpensive aspect of 3D visualization. We believe this approach will be quite effective for high-resolution observations of plant tissues or organs without the limits on sample type or size presented by other methods. Furthermore, the sample used in this work is permanently preserved and has inherent reproducibility, both physically and digitally, as long as the original slides are conserved and the digital files are carefully archived. The data are reproducible insofar as similar organs and tissues from plants of the same species grown in a comparable manner and prepared in the same way can be studied and compared using this method. We believe that this method offers an inexpensive option for the study of plant tissue structures of any type that can be sectioned, for use by any scientist with access to a microtome, a good microscope equipped with a digital camera, and a personal computer.

AUTHOR CONTRIBUTIONS

Y.M. designed the digital protocols for converting photomicrographic data into digital data suitable for constructing 3D virtual objects or analyzing tissue development, performed data analysis, and contributed to the manuscript. S.S. did photomicroscopy and data interpretation. T.N. developed the novel histological methods to prepare the plant material for microscopy, did data interpretation, and contributed to the manuscript. D.K.G did data interpretation, contributed to and prepared the manuscript for publication. All authors approved the final version of the manuscript.

DATA AVAILABILITY STATEMENT
All supporting data are available with the published article.

ORCID
Daniel K. Gladish http://orcid.org/0000-0001-5721-7532

REFERENCES

Bougourd, S., J. Marrison, and J. Haseloff. 2000. An aniline blue staining procedure for confocal microscopy and 3D imaging of normal and perturbed cellular phenotypes in mature *Arabidopsis* embryos. *Plant Journal* 24: 543–550.

Buda, J., T. Isaacson, A. J. Matas, D. J. Paolillo, and J. K. C. Rose. 2009. Three-dimensional imaging of plant cuticle architecture using confocal scanning laser microscopy. *Plant Journal* 60: 378–385.

Bussolati, G., C. Marchiò, and M. Volante. 2005. Tissue arrays as fiducial markers for section alignment in 3-D reconstruction technology. *Journal of Cellular and Molecular Medicine* 9: 438–445.

GIMP Development Team. 2018. GIMP. Website: https://www.gimp.org [accessed 9 June 2023].

Gladish, D. K., and T. Niki. 2000. Factors inducing cavity formation in the vascular cylinders of pea roots (*Pisum sativum* L., cv. 'Alaska'). *Environmental and Experimental Botany* 43: 1–9.

Glidewell, S. M. 2006. NMR imaging of developing barley grains. *Journal of Cereal Science* 43: 70–78.

Glidewell, S. M., B. Williamson, G. H. Duncan, J. A. Chudek, and G. Hunter. 1999. The development of blackcurrant fruit from flower to maturity: A comparative study by 3D nuclear magnetic resonance (NMR) micro-imaging and conventional histology. *New Phytologist* 141: 85–98.

Gray, J. D., P. Kolesik, P. B. Høj, and B. G. Coombe. 1999. Confocal measurement of the three-dimensional size and shape of plant parenchyma cells in a developing fruit tissue. *Plant Journal* 19: 229–236.

Gubatz, S., V. J. Dercksen, C. Brüß, W. Weschke, and U. Wobus. 2007. Analysis of barley (*Hordeum vulgare*) grain development using three-dimensional digital models. *Plant Journal* 52: 779–790.

Haase, R., E. Fazeli, D. Legland, M. Doube, S. Culley, I. Belevich, E. Jokitalo, et al. 2022. A hitchhiker's guide through the bio-image analysis software universe. *FEBS Letters* 596: 2472–2485.

Haseloff, J. 2003. Old botanical techniques for new microscopes. *BioTechniques* 34: 1174–1182.

Ishida, N., M. Koizumi, and H. Kano. 2000. The NMR microscope: A unique and promising tool for plant science. *Annals of Botany* 86: 259–278.

Kitin, P., Y. Sano, and R. Funada. 2003. Three dimensional imaging and analysis of differentiating secondary xylem by confocal microscopy. *IAWA Journal* 24: 211–222.

Lee, K., J. Avondo, H. Morrison, L. Blot, M. Stark, J. Sharpe, A. Bangham, and E. Coen. 2006. Visualizing plant development and gene expression in three dimensions using optical projection tomography. *Plant Cell* 18: 2145–2156.

Majumder, S., C. M. DeMott, S. Reverdatto, D. S. Burz, and A. Shekhtman. 2016. Total RNA modulates protein activity. *Biochemistry* 55: 4568–4573.

Miki, Y., S. Saito, T. Niki, and D. K. Gladish. 2020. Three-dimensional digital image construction of metaxylem vessels in root tips of *Zea mays* subsp. *mexicana* from thin transverse sections. *Applications in Plant Sciences* 8: e11347.

Mill, R. R., M. Moller, S. M. Glidewell, D. Masson, and B. Williamson. 2004. Comparative anatomy and morphology of fertile complexes of *Prumnopitys* and *Afrocarpus* species (Podocarpaceae) as revealed by histology and NMR imaging, and their relevance to systematics. *Botanical Journal of the Linnean Society* 145: 295–316.

Niki, T., D. K. Gladish, P. Lu, and T. L. Rost. 1995. Cellular changes precede cavity formation in the vascular cylinder of pea roots (*Pisum sativum* L. cv. 'Alaska'). *International Journal of Plant Sciences* 156: 290–302.

Niki, T., S. Saito, and D. K. Gladish. 2019. A novel thin section preparation and staining protocol to increase contrast and resolution of cell details for light microscopy. *Biotechnics and Histochemistry* 94: 522–526.

Ogawa, Y., H. Kuensting, J. Sugiyama, T. Ohtani, X. Q. Liu, M. Kokubo, K. Kudoh, and T. Higuchi. 2002. Structure of a rice grain represented by a new three-dimensional visualisation technique. *Journal of Cereal Science* 36: 1–7.

Ourselin, S., A. Roche, G. Subsol, X. Pennec, and N. Ayache. 2000. Reconstructing a 3D structure from serial histological sections. *Image and Vision Computing*, 19: 25–31.

Rasband, W. S. 1997–2014. ImageJ. U. S. National Institutes of Health, Bethesda, Maryland, USA. Website: http://imagej.nih.gov/ij/ [accessed 9 June 2023].

Saito, S., T. Niki, and D. K. Gladish. 2019. Comparison of promeristem structure and ontogeny of procambium in primary roots of *Zea mays* ssp. *mexicana* and *Z. mays* 'Honey Bantam' with emphasis on metaxylem vessel histogenesis. *Plants* 8: 162–177.

Stuppy, W. H., J. A. Maisano, M. W. Colbert, P. J. Rudall, and T. B. Rowe. 2003. Three-dimensional analysis of plant structure using high-resolution X-ray computed tomography. *Trends in Plant Science* 8: 2–6.

Truernit, E., H. Bauby, B. Dubreucq, O. Grandjean, J. Runions, J. Barthélémy, and J-C. Palauqui. 2008. High-resolution whole-mount imaging of three-dimensional tissue organization and gene expression enables the study of phloem development and structure in *Arabidopsis*. *Plant Cell* 20: 1494–1503.

Wegel, E., E. Pilling, G. Calder, S. Drea, J. Doonan, L. Dolan, and P. Shaw, 2005. Three-dimensional modelling of wheat endosperm development. *New Phytologist* 168: 253–262.

SUPPORTING INFORMATION

Additional supporting information can be found online in the Supporting Information section at the end of this article.

Video S1. Animated video of the 3D virtual reconstruction shown in Figure 6C.